Acoustic Propagation on Irrotational Mean Flows Using Transient Finite and Infinite Elements

James A. Hamilton[*] and R. Jeremy Astley[†]

University of Southampton, Southampton, England SO17 1BJ, United Kingdom

A formulation is presented for the computation of transient wave fields propagating on unbounded, irrotational mean flows. The numerical scheme is based on an inner mesh of conventional finite elements, which is matched to high-order multipole infinite elements in the far field. The scheme is validated against simple transient test solutions and shown to be effective for large three-dimensional problems provided that iterative solvers are used to advance the solution at each time step.

Nomenclature

a	=	characteristic length
$\boldsymbol{B}$	=	preconditioniong matrix
$\boldsymbol{C}$	=	acoustic damping matrix
$\mathcal{C}$	=	condition number
c_r	=	reference sound speed
$c_0(\boldsymbol{x})$	=	local sound speed
$F(\boldsymbol{x}, t)$	=	normal acoustic mass flux
$f(\boldsymbol{x}, \omega)$	=	acoustic mass flux amplitude
$\boldsymbol{G}$	=	transient forcing vector
$J_m()$	=	Bessel function of the first kind, order m
$\boldsymbol{K}$	=	acoustic stiffness matrix
$\hat{k}_r$	=	reference wave number, $= \omega/c_r$
M	=	freestream reference Mach number
$\boldsymbol{M}$	=	acoustic mass matrix
$M_0(\boldsymbol{x})$	=	local Mach number
p	=	acoustic pressure
$q_{ij}(\omega)$	=	trial coefficients for $\tilde{\phi}(\boldsymbol{x}, \omega)$
r, θ, φ	=	spherical polar coordinates
T	=	nondimensional time, $= ct/a$
t	=	time
U_r	=	freestream reference flow velocity
$U_0(\boldsymbol{x})$	=	local mean flow velocity
$\tilde{w}(\boldsymbol{x}, \omega)$	=	test function
$\tilde{w}_{ij}(\boldsymbol{x})$	=	test basis function
x, R, φ	=	cylindrical polar coordinates
β	=	Lorentz constant $= \sqrt{(1 - M^2)}$
Δt	=	time-step size
$\mu(\boldsymbol{x})$	=	phase function: trial solution
$\rho(\boldsymbol{x}, t)$	=	acoustic density perturbation
ρ_r	=	reference density
$\rho_0(\boldsymbol{x})$	=	local mean density
$\Phi(\boldsymbol{x}, t)$	=	acoustic velocity potential
$\phi(\boldsymbol{x}, \omega)$	=	acoustic velocity potential amplitude
$\tilde{\phi}(\boldsymbol{x}, \omega)$	=	trial solution for ϕ
$\tilde{\phi}_{ij}(\boldsymbol{x})$	=	trial basis function
$\psi(\boldsymbol{x})$	=	phase function: multipole expansion
ω	=	radian frequency

*Research Assistant, Institute of Sound and Vibration Research.
†Professor, Fluid Dynamics and Acoustics Group, Institute of Sound and Vibration Research. Member AIAA.

Introduction

FINITE element (FE) and infinite element (IE) models implemented in the frequency domain have proved an effective method for predicting acoustic radiation from axisymmetric turbofan inlets.[1,2] They require the assumption of an irrotational mean flow, but this is not unduly restrictive in the case of an inlet. With this proviso, they are able to deal well with the refractive effects of the mean flow, diffraction by the inlet geometry, and attenuation caused by liners. Such models are also readily matched to modal sound fields on the fan plane. When infinite elements are used in the far field, accurate far-field directivity functions are obtained directly from the computed solution without postprocessing.[3] Because only one dependent variable is needed at each node, such models are relatively inexpensive to run when compared to computational-aeroacoustics (CAA) models based on the Euler or linearized Euler equations. Indeed FE/IE codes can be used to optimize acoustic treatments of axisymmetrized inlets at acceptable computational cost for realistic frequencies, up to twice blade passing frequency (BPF), say at maximum power.[3] Such computations involve models of perhaps 50,000–100,000 degrees of freedom and can be performed in minutes rather than hours on a single processor.

The limitations of existing FE/IE models become apparent however when they are applied to fully three-dimensional problems. The FE/IE model requires the solution of a system of equations of the form

$$[\boldsymbol{A}(\omega)]\{\boldsymbol{q}\} = \{\boldsymbol{f}(\omega)\} \qquad (1)$$

where $[\boldsymbol{A}(\omega)]$ is a sparse matrix that is neither symmetric nor Hermitian. These equations do not lend themselves to robust iterative solution and are generally solved using direct methods, typically sparse or frontal solvers tailored to take advantage of the sparse nature of the coefficient matrix. This has the advantage of dealing efficiently with multimode excitation at little extra cost. This is particularly helpful in cases when broadband fan noise can be approximated by a multimode ensemble of uncorrelated cut-on modes of equal intensity, as is commonly the case. The reduction of the matrix need then only be performed once and the solution for each mode obtained by a backsubstitution at negligible computational cost. However, even when such economies are used, the solution times and memory requirements for the reduction phase of such solvers scale poorly with problem size and become impracticable for fully three-dimensional inlets at realistic frequencies, where the required number of grid points is likely to approach $10^6 - 10^7$. Indirect frequency-domain solvers have been implemented for three-dimensional FE/IE models[4] but have not been demonstrated to be effective for large problems with flow at realistic frequencies.

The formulation of the FE/IE equations in the time domain circumvents many of the preceding difficulties. This is the subject of the current paper. The method proposed still generates a large system of equations at each time step, but this can be treated effectively using Krylov subspace indirect solvers. The local nature

of the discrete transient problem at each time step rewards iterative schemes. This is so in the absence of preconditioning techniques, but can be enhanced by their use. Memory requirements are vastly reduced because only the nonzero terms of the coefficient matrix need to be stored.

In the current paper a general infinite element formulation is presented for time-domain flow acoustics. The scheme is validated by numerical studies of simple axisymmetric test problems. The effectiveness of using iterative solvers at each time step is then demonstrated for three-dimensional problems in the absence of flow. These studies confirm that CPU usage and memory requirements for such solutions are many orders of magnitude less than for equivalent frequency-domain models.

Geometry and Governing Equations

Transient Initial-Value Problem

Consider the sound field in an unbounded domain $R^e (\in \mathbb{R}^3)$ exterior to a convex surface Γ, which encloses any sound sources or reflecting surfaces. The region interior to Γ is denoted by R^i (Fig. 1). A steady mean flow within $R (= R^i \cup R^e)$ is represented by a velocity field $U_0(x)$, a mean density field $\rho_0(x)$, and an associated sound speed $c_0(x)$. At large distances from Γ, the mean flow is of magnitude U_r in the direction of the x axis. Corresponding reference values of density and sound speed are ρ_r and c_r. The local vector Mach number is defined as $M_0(x) = U_0(x)/c_0(x)$ and the freestream Mach number M as $M = U_r/c_r$. An acoustic disturbance is generated in R^i and propagates into R^e across the interface Γ. The mean flow and the acoustic perturbation are inviscid, irrotational, and isentropic. The acoustic velocity potential $\Phi(x, t)$ and the acoustic density perturbation $\rho(x, t)$ then satisfy the linearized inviscid continuity equation

$$\nabla \cdot (\rho_0 \nabla \Phi + \rho U_0) + \frac{\partial \rho}{\partial t} = 0 \qquad (x \in R^e, t \geq 0) \quad (2)$$

and a linearized version of the momentum equation

$$\rho = -\frac{\rho_0}{c_0^2}\left(\frac{\partial \Phi}{\partial t} + U_0 \cdot \nabla \Phi\right) \qquad (3)$$

Alternatively, the preceding equations can be combined to give a single second-order, convected wave equation

$$\frac{\partial}{\partial t}\left[\frac{\rho_0}{c_0^2}\left(\frac{\partial \Phi}{\partial t} + U_0 \cdot \nabla \Phi\right)\right]$$
$$- \nabla \cdot \left[\rho_0 \nabla \Phi - \frac{\rho_0}{c_0^2}\left(\frac{\partial \Phi}{\partial t} + U_0 \cdot \nabla \Phi\right)U_0\right] = 0 \quad (4)$$

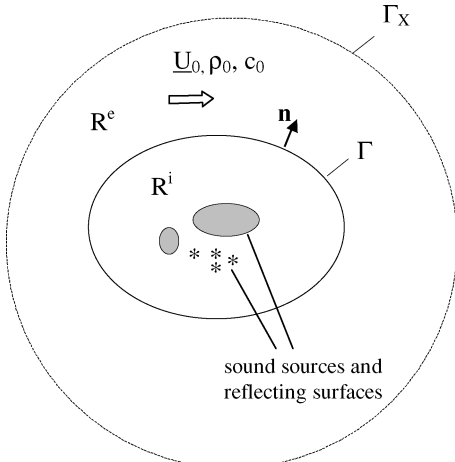which reduces to the simple wave equation for the case of a homogeneous medium with zero mean flow.

Fig. 1   Problem geometry.

We seek solutions for $\Phi(x, t)$ in the outer region R^e for $t \geq 0$ subject to the initial conditions

$$\Phi(x, 0) = \dot{\Phi}(x, 0) = 0, \qquad x \in R^e \quad (5)$$

The acoustical field within the inner region R^i will not be considered here in any detail. In the numerical studies to be presented later in this paper, it is modeled by a conventional finite element model of the type described by Eversman.[1] The analysis presented here will focus on the formulation of a numerical model for the outer region R^e and will assume that such a solution is weakly coupled to an inner FE model or to a prescribed acoustic mass flux normal to the interface Γ, that is, a condition of the form

$$(\rho_0 \nabla \Phi + \rho U_0) \cdot n = F(x, t), \qquad x \in \Gamma, \qquad t \geq 0 \quad (6)$$

where $F(x, t)$ is prescribed for $t > 0$. For the case of zero mean flow, this corresponds to the specification of a prescribed normal velocity on Γ.

Time-Harmonic Problem

Steady time-harmonic solutions for this problem can be sought of the form

$$\Phi(x, t) = Re[\phi(x, \omega)e^{i\omega t}] \quad (7)$$

Equation (4) then reduces to

$$-\left(i\omega\rho_0/c_0^2\right)(i\omega\phi + U_0 \cdot \nabla\phi)$$
$$- \nabla \cdot \left[\rho_0\nabla\phi - \left(\rho_0/c_0^2\right)(i\omega\phi + U_0 \cdot \nabla\phi)U_0\right] = 0 \quad (8)$$

and boundary condition (5) becomes

$$\left[\rho_0\nabla\phi - \left(\rho_0/c_0^2\right)(i\omega\phi + U_0 \cdot \nabla\phi)U_0\right] \cdot n = f(x, \omega), \qquad x \in \Gamma \quad (9)$$

where $F(x, t) = Re[f(x, \omega)e^{i\omega t}]$. The initial conditions in the transient problem are replaced in the frequency domain by the Sommerfield radiation condition

$$r\left[\frac{\partial \phi}{\partial r} + ik_r(\nabla\psi \cdot \hat{r})\phi\right] \to 0, \qquad r \to \infty \quad (10)$$

where r is a spherical polar radius, $\psi(x)$ is a convected phase function (to be discussed shortly), and $k_r(= \omega/c_r)$ is a reference wave number.

Alternatively $\phi(x, \omega)$ can be regarded as the complex Fourier transform of $\Phi(x, t)$. That is to say, if ϕ and Φ are related by the transform pair

$$\phi(x, \omega) = \mathcal{F}[\Phi(x, t)] = \int_{-\infty}^{+\infty} \Phi(x, t)e^{-i\omega t}\, dt \quad (11)$$

$$\Phi(x, t) = \mathcal{F}^{-1}[\phi(x, \omega)] = \frac{1}{2\pi}\int_{-\infty}^{+\infty} \phi(x, \omega)e^{+i\omega t}\, d\omega \quad (12)$$

and if $f(x, \omega)$ is similarly defined as the Fourier transform of $F(x, t)$, Eqs. (8) and (9) become the Fourier transforms of Eqs. (4) and (6).

Multipole Expansion for Uniform Flow

In the case of zero mean flow ($U_0 = 0$), it is known that any unbounded solution of Eq. (8) can be written as a multipole expansion

$$\phi(x, \omega) = \sum_{j=1}^{\infty} \frac{g_j(\omega, \theta, \varphi)}{r^j}e^{-ik_r r} \quad (13)$$

The preceding expression is uniformly convergent in the region exterior to a sphere that encloses all sound sources and reflecting surfaces.[5] By applying the Lorentz transformation to this result, it is not difficult to show that for the case of a uniform axial mean
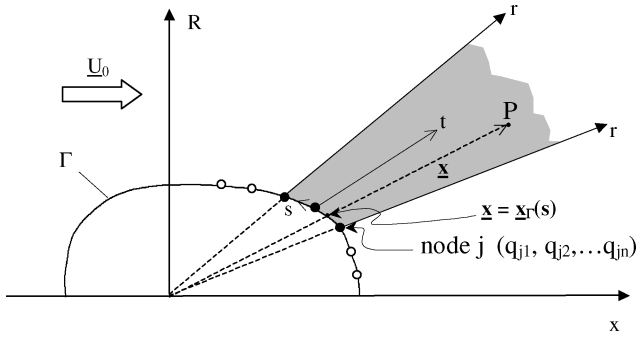
Fig. 2 Infinite element model.

flow $U_0(x) = c_r M \hat{x}$ an equivalent uniformly convergent expansion is given by

$$\phi(x, \omega) = \sum_{j=1}^{\infty} \frac{g_j(\omega, \theta, \varphi)}{r^j} \exp[-ik_r \psi(x)] \qquad (14)$$

where

$$\psi(x) = \frac{-Mx + \sqrt{x^2 + (1 - M^2)R^2}}{1 - M^2} \qquad (15)$$

and where R is a cylindrical polar radius. The surfaces $\psi = $ constant defined by expression (15) correspond to a family of convected phase surfaces for a simple stationary source at the origin. Expression (14) is then uniformly valid within a bounding spheroid, which encloses all sound sources and reflecting surfaces.

Infinite Element Model

An infinite element model for the outer domain R^e is formed by dividing it into radial segments as indicated in Fig. 2. Each segment forms a single element and is anchored to the inner surface Γ by a variable number of nodes. These determine the transverse interpolation order of the element; "linear" for an element with two base nodes, "quadratic" for an element with three base nodes, as shown in Fig. 2, and so on. Then, n degrees of freedom are defined at each node, say, $q_{j1}, q_{j2} \ldots q_{jn}$ at node j. The discretization of the outer region therefore involves $N = n \times m$ degrees of freedom, where m is the number of nodes on Γ and n is the number of degrees of freedom per node. The infinite edges of each element are aligned radially with respect to a spherical coordinate system whose origin can be defined independently for each node on Γ. In all that follows, a common global origin will be assumed for these nodal source points.

Trial Solution in Frequency Domain

The trial solution $\tilde{\phi}(x, \omega)$ within the infinite element region is defined as

$$\tilde{\phi}(x, \omega) = \sum_{i=1}^{n} \sum_{j=1}^{m} q_{ij}(\omega) \tilde{\phi}_{ij}(x) e^{-ik_r \mu(x)} \qquad (16)$$

The basis functions $\tilde{\phi}_{ij}(x)$ model the amplitude variation of the solution while the phase function $\mu(x)$ represents the local oscillatory component. The specification of these quantities for flow acoustics is guided by the form of expansion (14). The phase function $\mu(x)$ is defined in terms of the multipole phase function $\psi(x)$ of expansion (14). At a field point P (see Fig. 2) $\mu(x)$ is defined to be

$$\mu(x) = \psi(x) - \psi(x_\Gamma) \qquad (17)$$

where x_Γ is a point lying on the intersection of Γ with a radial line through P. This ensures that $\mu(x)$ takes the value of zero on the interface Γ. The basis functions $\tilde{\phi}_{ij}(x)$ are then formed so that along the radial edges they can be expanded in inverse powers of r. This is done by using an element mapping proposed originally by Bettess[6]

and applied to flow acoustics by Eversman.[1] The trial solution of expression (16) then duplicates the multipole expansion of expression (14) truncated after n terms. This guarantees approximability, but not necessarily convergence, as $n \to \infty$. The particular combinations of inverse polynomial terms in r, which are included in the functions $\tilde{\phi}_{ij}(x)$, have an effect on the conditioning of the discrete problem.[7] The hierarchical radial basis proposed by Shirron and Babuska[8] is known to give well-conditioned results for analagous treatments of no-flow problems. This has been used in the current instance and found to give well- conditioned equations.

Weak Formulation

A weak variational statement[9,10] of the problem posed by Eq. (8) and incorporating boundary conditions (9) and (10) requires that

$$\int_{R^e} \tilde{w} \left[-\frac{i\omega\rho_0}{c_0^2}(i\omega\tilde{\phi} + U_0 \cdot \nabla\tilde{\phi}) \right] dR^e$$

$$+ \int_{R^e} \nabla\tilde{w} \cdot \left[\rho_0 \nabla\tilde{\phi} - \frac{\rho_0}{c_0^2}(i\omega\tilde{\phi} + U_0 \cdot \nabla\tilde{\phi})U_0 \right] dR^e$$

$$- \lim_{X \to \infty} \int_{\Gamma_X} \tilde{w} \left[\rho_0 \nabla\tilde{\phi} - \frac{\rho_0}{c_0^2}(i\omega\tilde{\phi} + U_0 \cdot \nabla\tilde{\phi})U_0 \right] \cdot \hat{r}\, d\Gamma_X$$

$$+ \int_{\Gamma} \tilde{w} f(x, \omega)\, d\Gamma = 0 \qquad (18)$$

for all permissible test functions $\tilde{w}(x, \omega)$. In the current instance these functions are chosen as

$$\tilde{w}(x, \omega) = \tilde{w}_{ij}(x) e^{+ik\mu(x)} \qquad (19)$$

where

$$\tilde{w}_{ij}(x) = (r_\Gamma/r)^2 \tilde{\phi}_{ij}(x) \qquad (20)$$

This choice arises naturally in the no-flow case from a variational setting proposed by Leis[11] but can also be derived from physical considerations.[12] In effect, it involves multiplying the complex conjugate of each trial basis function by a geometric factor $(r_\Gamma/r)^2$.

When expressions (16) and (19) are substituted into Eq. (18), a set of linear equations results of the form

$$\left(K_{ijkl} + i\omega C_{ijkl} - \omega^2 M_{ijkl} \right) q_{kl} + f_{ij}(\omega) = 0 \qquad (21)$$

where K, C, and M are frequency-independent arrays whose components are given by

$$K_{ijkl} = \int_{R^e} \rho_0 \{ \nabla\tilde{w}_{ij} \cdot \nabla\tilde{\phi}_{kl} - (M_0 \cdot \nabla\tilde{w}_{ij})(M_0 \cdot \nabla\tilde{\phi}_{kl}) \}\, dR^e \quad (22)$$

$$C_{ijkl} = \int_{R^e} \left\{ \frac{\rho_0}{c_r}(\tilde{w}_{ij}(\nabla\tilde{\phi}_{kl} \cdot \nabla\mu) - (\nabla\tilde{w}_{ij} \cdot \nabla\mu)\tilde{\phi}_{kl}) \right.$$

$$+ \left(\frac{\rho_0}{c_0} - \frac{\rho_0}{c_r}M_0 \cdot \nabla\mu \right)$$

$$\left. \times (\tilde{w}_{ij}M_0 \cdot \nabla\tilde{\phi}_{kl} - M_0 \cdot \nabla\tilde{w}_{ij}\tilde{\phi}_{kl}) \right\} dR^e \qquad (23)$$

$$M_{ijkl} = \int_{R^e} \frac{\rho_0}{c_0^2} \left\{ 1 - 2\frac{c_0}{c_r}M_0 \cdot \nabla\mu - \left(\frac{c_0}{c_r} \right)^2 \nabla\mu \cdot \nabla\mu \right.$$

$$\left. + \left(\frac{c_0}{c_r} \right)^2 (M_0 \cdot \nabla\mu)^2 \right\} \tilde{w}_{ij}\tilde{\phi}_{kl}\, dR^e \qquad (24)$$

The components of the forcing vector f_{ij} are frequency dependent, being given by

$$f_{ij}(\omega) = \int_{\Gamma} \tilde{w}_{ij} f(x, \omega)\, d\Gamma \qquad (25)$$

All of the preceding integrals are performed locally within each element and assembled in the usual way. Equation (21) can then be solved to give the unknown coefficients $q_{ij}(\omega)$, which define an approximate solution for the time-harmonic problem at all points in the outer domain. This is the frequency-domain infinite element formulation for the flow case.[1]

Transformation to Time Domain

Because the arrays K, M, and C are frequency independent, Eq. (21) can be transformed quite simply to the time domain. This gives a discrete system of transient equations of the form

$$K_{ijkl}Q_{kl} + C_{ijkl}\dot{Q}_{kl} + M_{ijkl}\ddot{Q}_{kl} = F_{ij}(t) \qquad (26)$$

where $Q_{kl}(t) = \mathcal{F}^{-1}[q_{kl}(\omega)]$ and

$$F_{ij}(t) = \mathcal{F}^{-1}[f_{ij}(\omega)] = \int_{\Gamma}[\tilde{w}_{ij}F(\boldsymbol{x},t)]\,\mathrm{d}\Gamma \qquad (27)$$

Equations (26) when solved subject to initial conditions $Q_{ij}(0) = \dot{Q}_{ij}(0) = 0$ form a discrete model for the initial value problem posed by Eqs. (4–6). When integrated in time, they give a solution $Q_{kl}(t)$ for a given surface excitation $F(\boldsymbol{x},t)$. The full transient solution at any exterior field point, $\boldsymbol{x}_P$ say, can then be reconstructed by taking the Fourier transform of expression (16) and applying the shift theorem to give

$$\tilde{\Phi}(\boldsymbol{x}_P,t) = \sum_{j=1}^{n}\sum_{k=1}^{m}\tilde{\phi}_{jk}(\boldsymbol{x}_P)Q_{jk}[t-\mu(\boldsymbol{x}_P)/c_r] \qquad (28)$$

that is, the transient solution at any point in the outer domain is obtained by interpolating the delayed time histories at neighboring nodes. It is simple to show that in the case where the field point is a node on Γ, that is, $\boldsymbol{x}_P = \boldsymbol{x}_j$, Eq. (28) reduces to

$$\tilde{\Phi}(\boldsymbol{x}_j,t) = Q_{j1}(t) \qquad (29)$$

Solving the Transient Equations

Although two indices k and l ($k = 1\ldots n, l = 1\ldots m$) have been used to define the unknown parameters $q_{kl}(\omega)$ and $Q_{kl}(t)$, these latter variables are readily reindexed as vectors with N components, where $N = mn$. Similarly, K, C, and M can be rewritten as $N \times N$ matrices, and Eq. (26) becomes a second-order system of linear equations of the form

$$[K]\{Q\} + [C]\{\dot{Q}\} + [M]\{\ddot{Q}\} = F(t) \qquad (30)$$

These are identical in form to the discrete equations that arise in linear structural dynamics. A wide range of explicit and implicit time-stepping schemes are available for the solution of such equations. Because there is no obvious way of lumping the mass and damping matrices without destroying the nonreflecting properties of the infinite elements, there is little attraction in using an explicit scheme. In the current instance an implicit Newmark scheme ($\beta = \frac{1}{4}, \gamma = \frac{1}{2}$, the average acceleration method) has been used. This is nondissipative and unconditionally stable. The algorithm at each time step is given by

$$A\ddot{Q}_{t+\Delta t} = G_{t+\Delta t} \qquad (31a)$$

$$\dot{Q}_{t+\Delta t} = \dot{Q}_t + \Delta t[(1-\gamma)\ddot{Q}_t + \gamma\ddot{Q}_{t+\Delta t}] \qquad (31b)$$

$$Q_{t+\Delta t} = Q_t + \Delta t\dot{Q}_t + (\Delta t^2/2)[(1-2\beta)\ddot{Q}_t + 2\beta\ddot{Q}_{t+\Delta t}] \qquad (31c)$$

where the subscripts t and $t+\Delta t$ denote the solution at successive time steps. The matrix A is a time-independent transient coefficient matrix, and $G_{t+\Delta t}$ is a time-dependent transient forcing vector; these are given by

$$A = M + \gamma\,\Delta t\,C + \beta\,\Delta t^2 K \qquad (32a)$$

$$G_{t+\Delta t} = F_{t+\Delta t} - C[\dot{Q}_t + (1-\gamma)\Delta t\ddot{Q}_t]$$

$$\qquad - K\big[Q_t + \Delta t\dot{Q}_t + (\Delta t^2/2)(1-2\beta)\ddot{Q}_t\big] \qquad (32b)$$

The bulk of the computational work at each time step lies in the solution of the linear system of equations (31a). When a direct solver is used, the factorization or reduction of A is performed once only at the first time step, and the solution at each subsequent time step is then given by the relatively inexpensive process of forward/backward substitution.

Alternatively, Eq. (31a) can be solved at each time step using an iterative method. This is more attractive in the time domain than in the frequency domain. In the time domain, the discrete solution is local in the sense that each nodal value is influenced only by neighboring points within a radius $c\Delta t$. This property is rewarded by an iterative scheme as is the availability of a good initial guess from the preceding time step.

In this paper, Krylov subspace iterative solvers are used to treat Eq. (31a). Specifically the generalized minimum residual (GMRES)[13] and the biconjugate gradient stabilized (Bi-CGSTAB)[14] methods are applied.

The convergence rates of iterative schemes can be improved by the introduction of preconditioning. This process maps the original linear system according to

$$B^{-1}A\ddot{Q}_{t+\Delta t} = B^{-1}G_{t+\Delta t} \qquad (33)$$

where B is the preconditioning matrix. Two simple forms of preconditioning have been used in the current study; diagonal preconditioning in which $B = \mathrm{diag}(A)$ and zero fill-in incomplete lower/upper factorization [ILU(0)].

Results

The results to be presented here will demonstrate first that time-domain infinite elements can deal accurately with convective mean flow propagation effects, and second that they offer significant potential savings in terms of CPU usage and storage for the solution of large three-dimensional time-harmonic problems.

General Validation of Transient Formulation for Flow Problems

Benchmark solutions generated from prescribed source distributions in uniform flows will be used to validate the current scheme. Such solutions can be constructed quite simply either in the frequency or time domains to give known sound fields of arbitrary complexity. A test problem of this type is shown in Fig. 3. Two monopole sources S1 and S2 lie a distance d apart in a uniform axial flow of Mach number M. They are enclosed by a spherical surface Γ through which the mean flow passes unimpeded. An infinite element mesh entirely fills the region exterior to Γ as indicated in Fig. 3. The origin of the elements is chosen so that Γ forms a convected phase surface $\psi(\boldsymbol{x}) = $ constant. This ensures that the discrete transient equations are stable in time.[2] An acoustic mass flux consistent with the sound field generated by the sources at S1 and S2 is then applied on Γ. The exterior solution computed from the infinite element model can then be compared to the analytic solution. This procedure allows for precise measurement of numerical error over a range of frequencies and Mach numbers. In the results that follow, the solution is sampled at surface points on Γ, such as A and B, (Fig. 3), and also at corresponding far-field points A' and B' obtained by projecting A and B outward by a radial factor of 10.0.
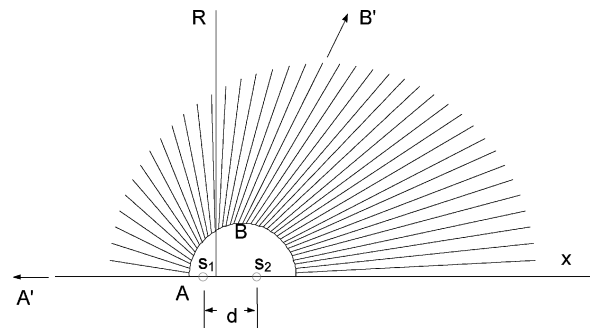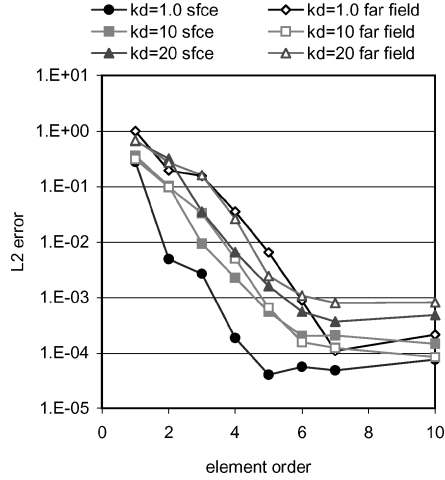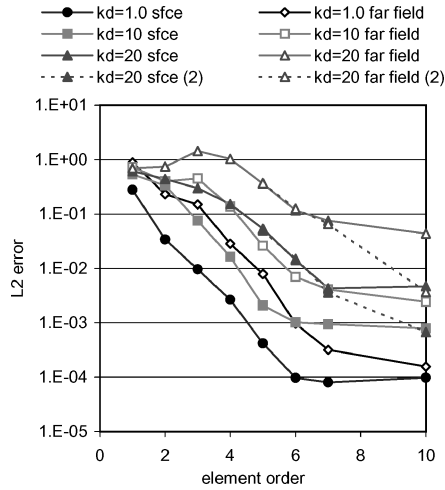
Fig. 3 Test problem and IE mesh.

A composite surface error ϵ is defined by summing the absolute error in the solution at all nodal points on Γ to give

$$\epsilon = \left[\frac{\sum_{j=1}^{m} \left| \phi^j - \phi_e^j \right|^2}{\sum_{j=1}^{m} \left| \phi_e^j \right|^2} \right]^{\frac{1}{2}} \tag{34}$$

where ϕ^j and ϕ_e^j are the computed and exact values of the solution at node j. A similar error is defined for the corresponding far-field

a) $M = 0.0$

b) $M = 0.5$

Fig. 4   Test problem: frequency-domain solution. Convergence with element order for a) $M = 0$ and b) $M = 0.5$.

points. These are relatively severe measures of error, which include discrepancies in phase as well as in the absolute value of the solution. This is important at higher frequencies, where phase error arises in conventional finite element models as a result of the so-called "pollution" effect.[15,16]

Results are presented for elements of variable radial order. Quadratic variation is assumed in the transverse direction. In all cases the sources at S1 and S2 are excited with equal strengths but with a phase difference of 180 deg, so that the resulting sound field is dipole like at low frequencies. A sinusoidal pulse is used for the transient excitation.

Spatial Resolution: Effect of Radial Element Order

The frequency-domain infinite element scheme and the time-domain infinite element scheme involve identical spatial discretizations. Solutions of the frequency-domain benchmark problem can therefore be used to investigate mesh resolution for either model. Convergence data for the test problem of Fig. 3 solved in the frequency domain for steady time-harmonic excitation are shown in Fig. 4 for Mach numbers of zero and 0.5. Here the surface and far-field errors given by Eq. (34) are plotted against infinite element order for frequencies in the range $kd = 1.0$ to $kd = 20$. A mesh of 40 equally spaced elements is used. The near- and far-field errors decrease with infinite element order, stabilizing when all significant mutipole contributions have been modeled (at around order five or six in most cases). The error generally increases with frequency and Mach number, as one would expect given that the characteristic wavelength of the solution decreases with frequency and is further compressed in the forward quadrant by an adverse Mach number. Solution accuracy can however be improved by increasing the number of elements, as illustrated by the additional data shown in Fig. 4b. This is obtained by doubling the number of elements, to 80, for the most demanding case ($kd = 20$, $M = 0.5$). The quality of the solutions obtained for the low-frequency ($kd = 1.0$) and high-frequency ($kd = 20.0$) cases is illustrated in Fig. 5 for $M = 0.5$. Here computed and exact instantaneous contours of velocity potential are plotted in the upper and lower half-planes of each figure. The computed values are obtained from the 40 element mesh of Fig. 3 with infinite elements of order 10. The exact and computed solutions are for all intents and purposes indistinguishable, emphasizing the demanding nature of the error parameter used in Fig. 4.

Accuracy of Transient Scheme

The convergence data of Fig. 4 indicate that the mesh of Fig. 3 with elements of order 10 should deal accurately with transient excitations for reduced frequencies in the range $kd \in [1.0, 20.0]$ and Mach numbers ≤ 0.5. Transient solutions obtained by solving the equivalent time-domain discrete equations [Eqs. (26)] are shown in Fig. 6. The sound field excited on Γ is generated by transient monopole sources at S1 and S2, which emit modulated sinusoidal
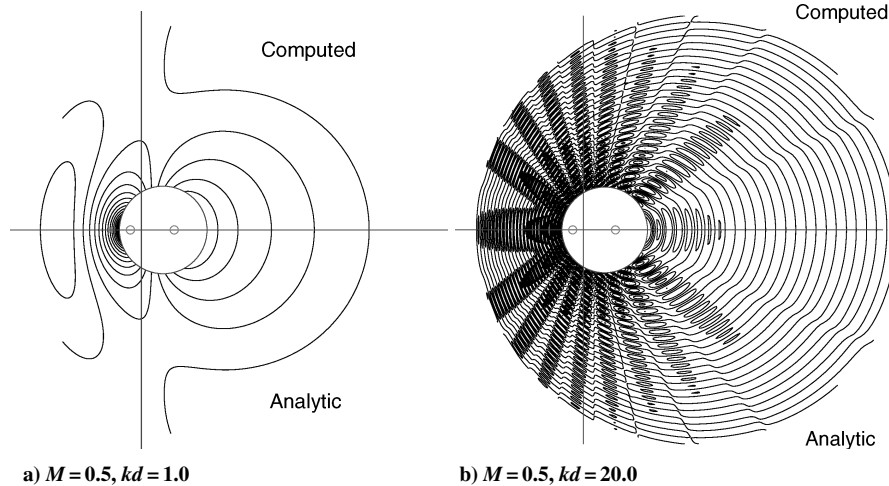

a) $M = 0.5$, $kd = 1.0$ **b)** $M = 0.5$, $kd = 20.0$

Fig. 5   Test problem: contours of instantaneous velocity potential. Frequency-domain solution.

a) $\omega = c_r/d$ $(kd = 1.0)$

b) $\omega = 20c_r/d$ $(kd = 20.0)$

c) $\omega = c_r/d$ $(kd = 1.0)$
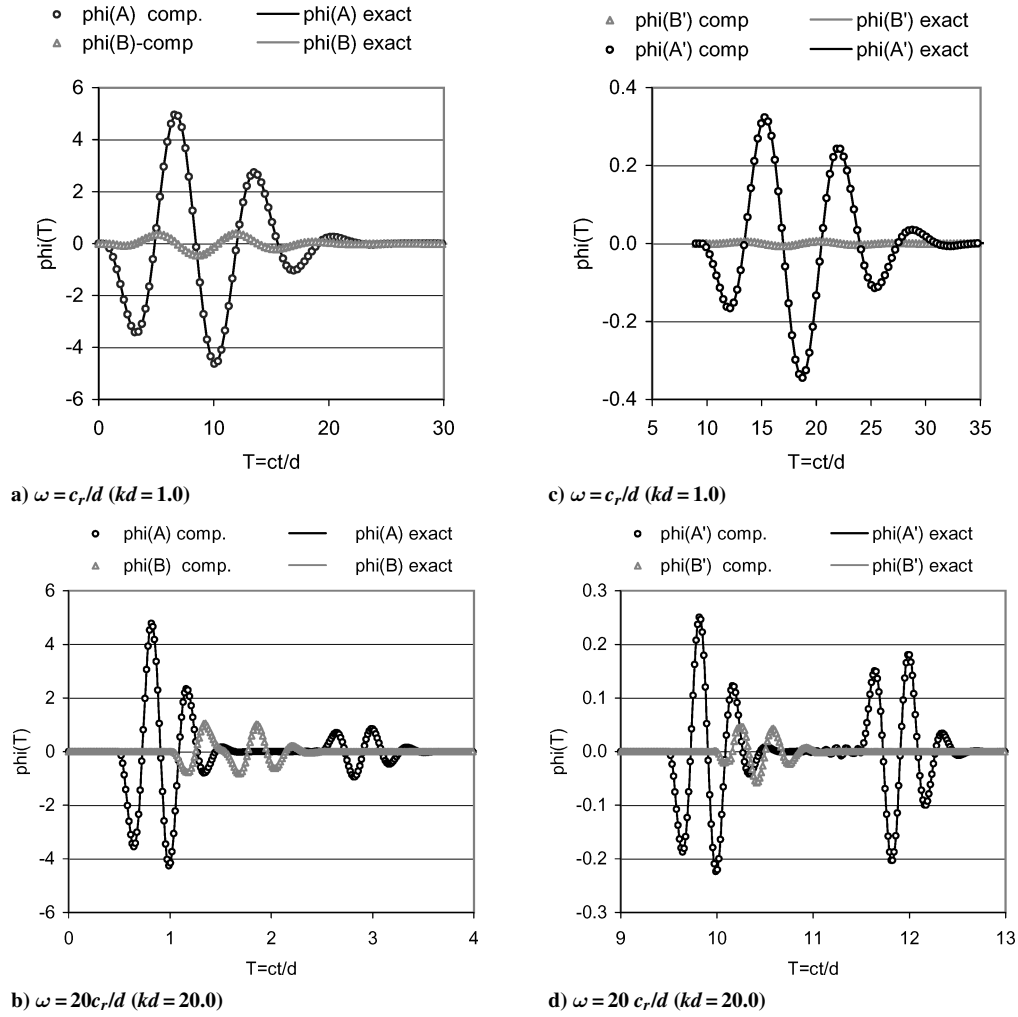
d) $\omega = 20\ c_r/d$ $(kd = 20.0)$

Fig. 6 Transient test problem: near- and far-field time histories. Gaussian pulse, $M = 0.5$.

pulses with carrier frequencies that correspond to reduced frequencies of $kd = 1.0$ and 20.0. The duration of the pulse is approximately four cycles.

A comparison of the exact and computed time histories at points A and B on the inner boundary of the mesh (see Fig. 3) is shown in Figs. 6a and 6b. The time step in each case is $1/20$ of the period of the carrier signal. At the lower frequency ($\omega = c_r/d$) the resulting sound field is essentially that of a dipole pulse, the transit time between the sources being small compared to the carrier period. At the higher frequency ($\omega = 20c_r/d$) the transit time between the sources is large, and a more complex sound field exists, two distinct pulses being evident at A while both signals arrive at B at approximately the same time. At both frequencies however the computed and exact solutions are virtually indistinguishable.

The same is true in the far field as indicated in Figs. 6c and 6d. These show similar time histories at A' and B'. In the case of Fig. 6d, the disturbance has traveled the equivalent of 30 carrier wavelengths, but no significant dissipation or dispersion error is apparent in the computed solution.

The time step used to obtain the results shown in Fig. 6 is small compared to the dominant frequency of the pulse. The numerical error associated with the discretization in time is therefore small.

The effect of varying the time step is illustrated in Fig. 7. Here the far-field time history at point A' is calculated using time steps $(1/20)T_f$, $(1/5)T_f$ and $(1/3)T_f$, where T_f is the period of the carrier frequency. Results are shown for the case $\omega = 20c_r/d$ for a time interval corresponding to the arrival of the first pulse. As the step size increases, some accuracy is lost, but stability is preserved. All but the first of these time increments exceeds the stability limit for an explicit scheme based on node spacing on the inner boundary Γ.
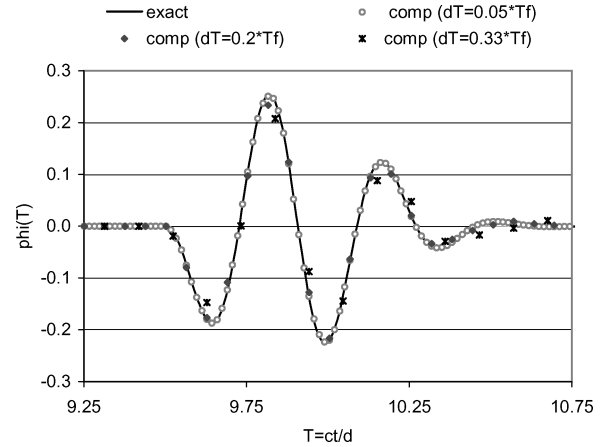

Fig. 7 Effect of time-step size on solution accuracy: time history at A', $\omega = 20c_r/d$ $(kd = 20.0)$.

General Comments

The results presented so far are trivial in the sense that they involve only small meshes and simple geometries. They serve to indicate, however, that established criteria that determine the accuracy of frequency-domain infinite elements in flow acoustics[3] carry over to the time-domain implementation. To be of practical use for large problems, the discrete equations in time must, however, be solved efficiently without matrix inversion. This option is studied in the next section.

Table 1 Number of FE nodes against geometry and $k_r a$

Geometry	Design kR					
	5	10	15	20	25	30
	1,089	7,361	23,425	60,672	113,756	191,224
	2,057	14,289	45,913	119,611	224,867	378,699
	3,881	27,729	89,977	235,789	444,485	——
	7,314	53,794	176,306	464,778	——	——

a) $\frac{1}{8}$-sphere model

b) $\frac{1}{4}$-sphere model
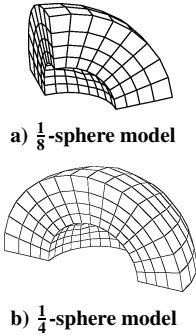
Fig. 8 Three-dimensional performance tests, spherical radiation models.

Performance Assessment of Iterative Solvers

Introduction

Results are presented now to demonstrate the use of iterative schemes in solving the transient equations at each time step. Zero-flow test problems are used in which infinite elements are attached to an inner finite element mesh, which is driven by a prescribed surface displacement at an inner boundary. The computational effort involved in obtaining solutions for steady time-harmonic excitation is compared to that required by direct solution in the frequency domain. The relative performance of different iterative and preconditioning schemes is assessed, as is the effect of IE order on conditioning and convergence.

Test-Problem Specification

The transient sound field generated by a vibrating spherical surface is used as a test problem. A quadrupole sound field is generated by setting the term $F(x, t)$ of Eq. (6) to

$$F(x, t) = P_2(\cos \varphi) \sin(\omega t) \qquad (35)$$

on the surface of a sphere at $r = a$, where $P_2()$ is a second-order Legendre polynomial. A finite element mesh encloses the vibrating surface and extends to a spherical interface of radius $2a$, where it is matched to a compatible mesh of infinite elements. Different models of similar resolution are then generated by employing symmetry conditions. Two of these are shown in Fig. 8, and the remainder are indicated in the first column of Table 1. Hexahedral elements with 20 nodes are used for the inner FE mesh, and resolution is set at 7–10 grid points per wavelength. Solutions are considered for reduced frequencies in the range $ka = 5$ to 30 giving model sizes which range from 1000 to 500,000 degrees of freedom (see Table 1). In all cases the time step is set to one-fifteenth of the period of the steady excitation. The transient solution was advanced until a steady time-harmonic state had been reached. This was achieved by continuing the transient calculation for three cycles after the solution had reached the FE/IE boundary.

Comparing Computational Effort for Time-Domain and Frequency-Domain Solutions

Frequency-domain solutions were performed for the test problem by using the FE/IE code ACTRAN-AE,[17] which solves Eq. (21) by using a sparse, out-of-core, direct solver. Solution times (performed on a PIII, 1-GHz machine with 1-GB RAM) for the frequency-domain solution and for the current time-domain iterative scheme are plotted against problem size in Fig. 9. The data for the direct
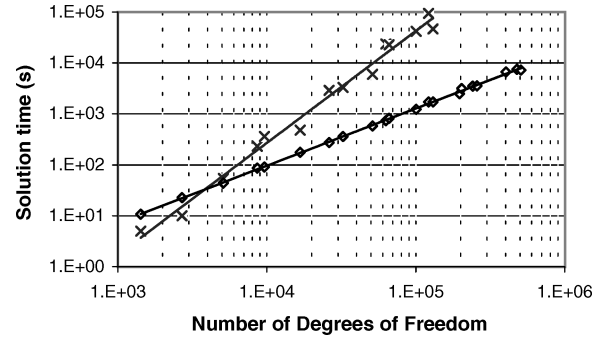
Fig. 9 Problem size against solution time: ×, ACTRAN; ——, ACTRAN fit; ◇, iterative; and ——, iterative fit.
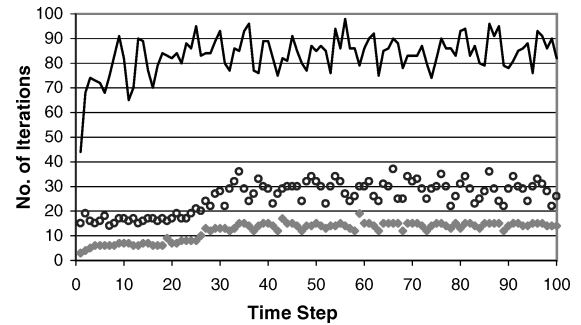
a) IE order 3
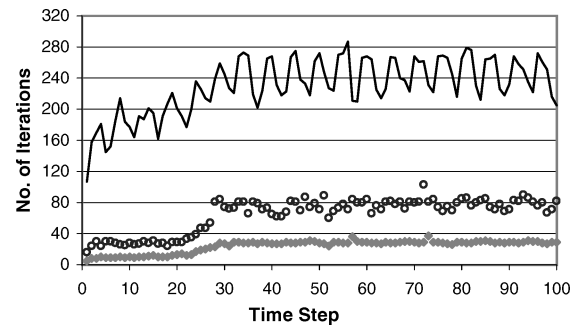
b) IE order 10

Fig. 10 Response of BiCGSTAB to preconditioning: ——, none; ○, diagonal; and ◆, ILU(0).

solver terminate when the out-of-core solver has consumed the available hard drive space ($\sim$25 GB in the current instance). The data for the iterative solver, which has no out-of-core capability, terminate when the available RAM is exceeded ($\sim$840 MB). It is a major advantage of the time-domain scheme that only the nonzero terms of the matrices need to be stored. The solution times for the transient scheme also scale with problem size at a much slower rate than for the direct solver. Lines of best fit show that the direct solver solution time scales as $t_s = (4.35 \times 10^{-7})N^{2.20}$, where t_s is the solution time and N is the problem size. For the iterative scheme the solution time scales as $t_s = (3.08 \times 10^{-3})N^{1.12}$.

Response to Preconditioning

Figure 10 illustrates the number of iterations per time step for different preconditioning regimes [no preconditioning, diagonal preconditioning and ILU(0)]. The $\frac{1}{8}$-sphere model was used with $k_r a = 15$ and the solution was advanced for 100 time steps. When infinite elements of order 3 were used, the equations were well conditioned giving a condition number $C = O(10^3)$. When elements of order of 10 were used, the condition number increased to $C = O(10^5)$. The results of Fig. 10 confirm that a larger number of iterations are required at the higher condition number. They show also that simple diagonal preconditioning offers a substantial improvement over the nonpreconditioned system, reducing the required number
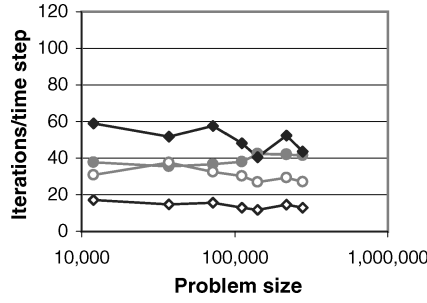
a) IE order 5
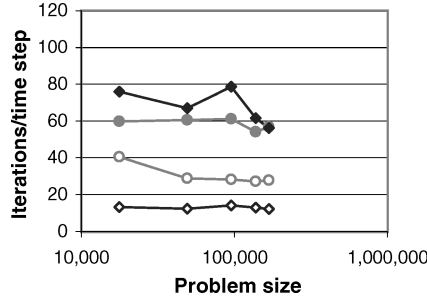
b) IE order 10
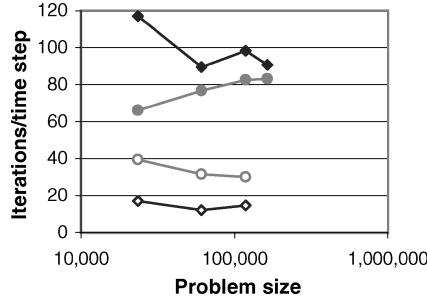
c) IE order 15

Fig. 11   GMRES vs BiCGSTAB, iterations: ◆, BiCGSTAB/diagonal: ◇, BiCGSTAB/ILU(0); ●, GMRES/diagonal; and ○, GMRES/ILU(0).
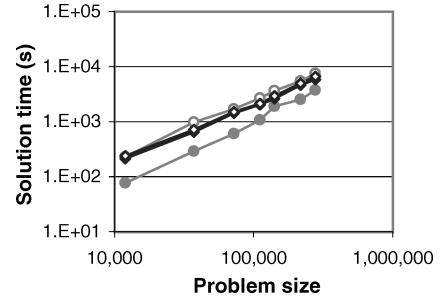

a) IE order 5

b) IE order 10

c) IE order 15

Fig. 12   GMRES vs BiCGSTAB, solution times: ◆, BiCGSTAB/ diagonal; ◇, BiCGSTAB/ILU(0); ●, GMRES/diagonal; and ○, GMRES/ILU(0).

of iterations by a factor of 3 in both cases. ILU(0) preconditioning further reduces the required iteration count, by a factor of about 2, and tends to reduce the variability from step to step. Note also the increase in the iteration count as the disturbance reaches the FE/IE boundary, at about time step 30. It is clear that the iterative procedure does not "see" the more poorly conditioned infinite elements until the disturbance actually reaches them.
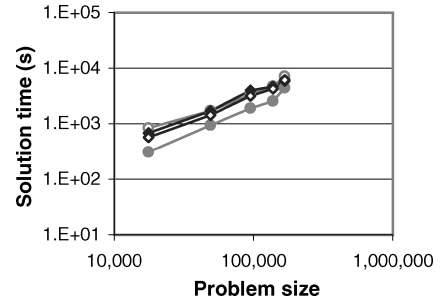
Comparison of BiCGSTAB and GMRES

A comparison of iteration counts for Bi-CGSTAB and GMRES is shown in Fig. 11. Results are shown for infinite elements of order 5, 10, and 15. Bi-CGSTAB requires more iterations than GMRES when diagonal preconditioning is used but responds better to ILU(0). When overall solution times are considered, however (Fig. 12), the performance of all solvers and preconditioners is comparable, indicating that the advantage of performing fewer iterations is offset in all cases by increased computational overheads at each iteration. Note however that the implementation of these methods might not be optimal and the preceding comments must therefore be regarded as preliminary. Nevertheless, it is encouraging that increasing the infinite element order has little effect on the overall rate at which the solution times scale with problem size.
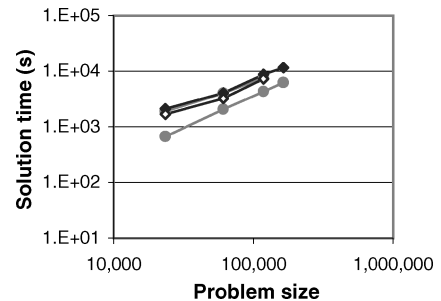
Demonstration Problem

Finally, the transient scheme is applied to a more realistic demonstration problem. The scheme is used to predict tone radiation from a representative negatively scarfed inlet. Zero mean flow is assumed. The problem is inherently three dimensional. The objective here is

simply to demonstrate that the current scheme is capable of generating near- and far-field results at frequencies of interest, for reasonable computational cost.

Geometry

The dimensions and geometry of the inlet are shown in Figs. 13a and 13b. The scarf angle is 10 deg. An artificial spherical baffle has been placed in the rear arc to close the computational domain.

Acoustic Input

The propagation of a rotor-alone tone in the inlet is simulated by prescribing an acoustic pressure on the fan plane characteristic of a high-order, propagating mode, that is, by an acoustic pressure distribution of the form[18,19]

$$P_{mn}(\boldsymbol{x}, t) = p_{mn}^0 J_m(k_{Rmn}R) \sin(m\theta + \omega t) \qquad (36)$$

where $J_m()$ is a Bessel function of the first kind, p_{mn}^0 is the mode amplitude (set at 1.0), and k_{Rmn} is the radial wave number. (R, φ, x) are cylindrical coordinates centered at the fan plane and aligned with the duct axis. The forcing term is weighted by the factor $\omega t/2\pi$ for $0 \le t \le 2\pi/\omega$ to ensure a nonimpulsive input to the time-domain problem. The frequency was taken to be 750 Hz, giving $ka = 17$, where a is the radius of the fan, and m and n are taken to be 13 and 1, respectively. These parameters are not unlike those of a buzz-saw tone tone at say half-BPF in a modern high-bypass-ratio turbofan engine at takeoff or cutback.
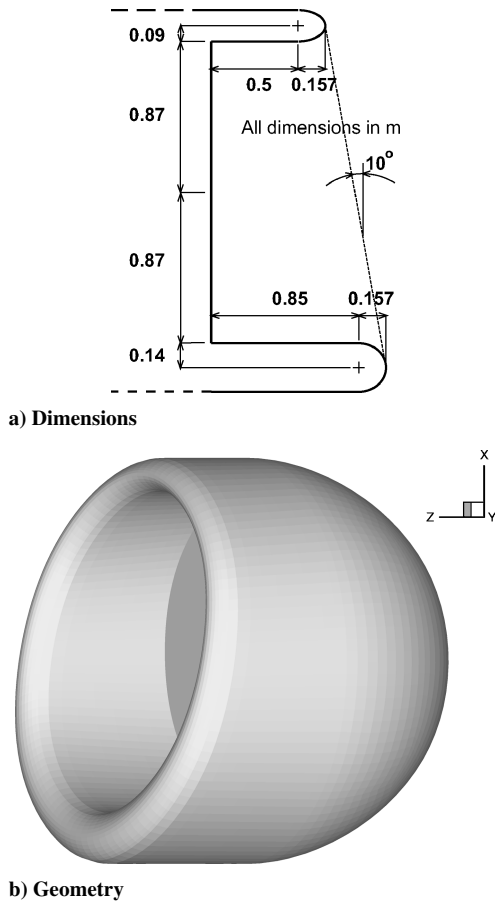
a) Dimensions

b) Geometry

Fig. 13   Geometry of the representative negatively scarfed inlet.

a) Slice through *x–z* plane

b) Surface mesh

Fig. 14   Finite element mesh.
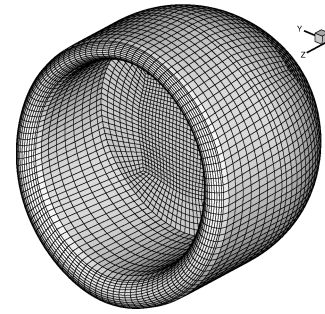
Finite/Infinite Element Model

The inner finite element mesh was created using quadratic, 20-node hexahedral elements. A slice of the mesh though the x–z plane and the projection of the mesh on the surface on the inlet are illustrated in Figs. 14a and 14b. The FE region was truncated by a spherical boundary of radius 1.5 m, centered 0.2 m ahead of the fan plane. Infinite elements of order 5 were used. The full model, including the infinite element mesh, contained approximately 450,000 degrees of freedom. The Bi-CGSTAB algorithm was used with diagonal preconditioning. A steady harmonic solution was obtained after 200 time steps. The complete solution required approximately 10 CPU hours on a single 1 GHz processor and 800 MB of in-core memory. Approximately 100 iterations were needed at each time step.

Results

Surfaces of constant acoustic pressure as the disturbance propagates along the inlet duct are shown in Fig. 15. They are plotted at nondimensional times $T = 1, 2,$ and 3, where $T = ct/a$. The corresponding pressure contours on the surface of the nacelle and on the FE/IE boundary are shown in Figs. 16 and 17. The final plot in Fig. 17, Fig. 17c at $T = 4$, represents the final steady-state solution. The current model clearly predicts that the acoustic radiation is directed slightly upwards in the near field, as one might expect given the geometry of the negative scarf. Far-field directivity can also be obtained from the numerical solution by applying expression (28). The resulting steady-state, far-field directivity functions in the vertical and horizontal planes are shown in Fig. 18. These are plots of the far-field acoustic pressure against angular coordinate in the $y = 0$ and $x = 0$ planes. (The coordinate system and slicing planes are illustrated in Fig. 19.) These results indicate that in the vertical plane, a small ($\sim$3 dB) reduction in peak acoustic pressure occurs in the downward direction.
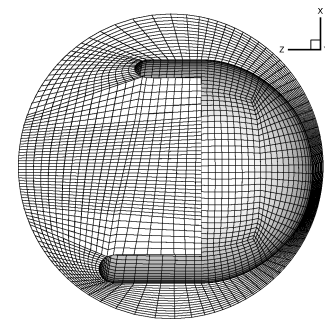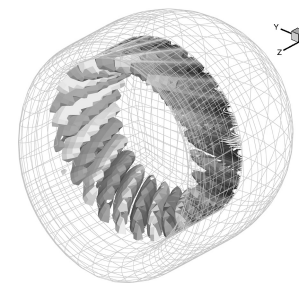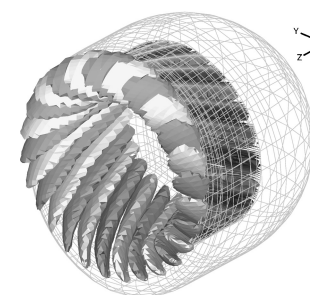

a) *T* = 1

b) *T* = 2
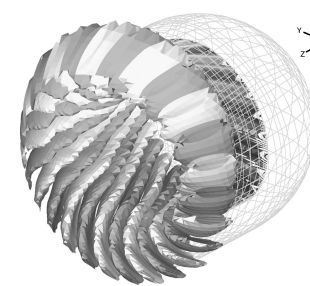
c) *T* = 3

Fig. 15   Pressure isosurfaces in the FE region.

a) $T = 1$ b) $T = 2$ c) $T = 3$
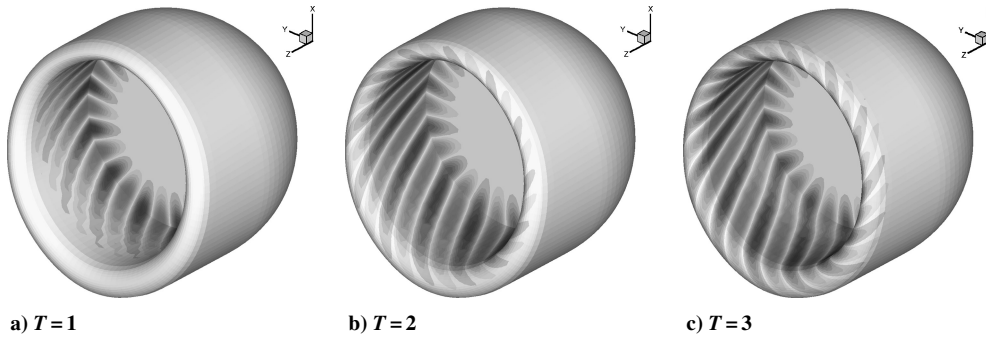
Fig. 16   Surface-pressure contours.

a) $T = 2$ b) $T = 3$ c) $T = 4$
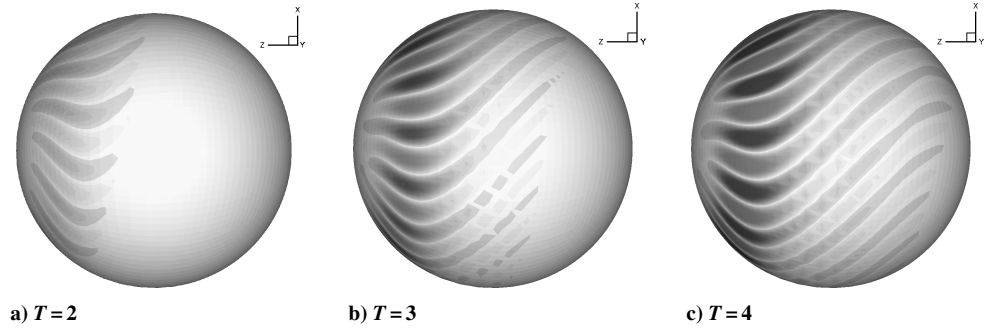
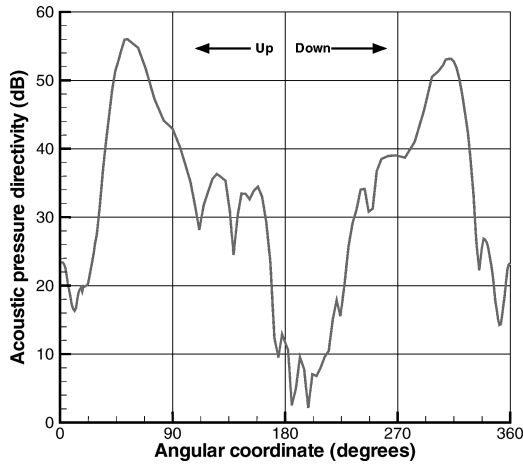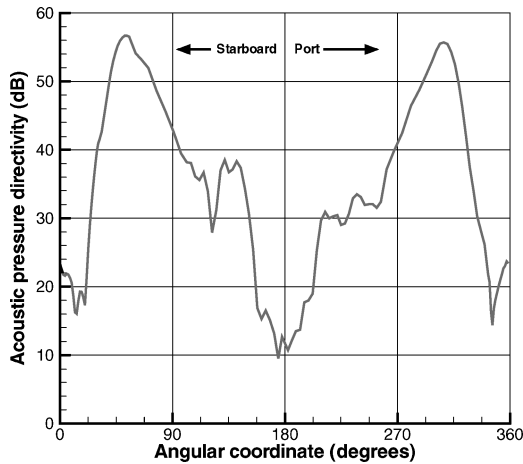Fig. 17   Pressure contours on the FE/IE boundary.

a) $y = 0$ $(z–x$ plane)

b) $x = 0$ $(y–z$ plane)

Fig. 18   Far-field acoustic pressure directivity.
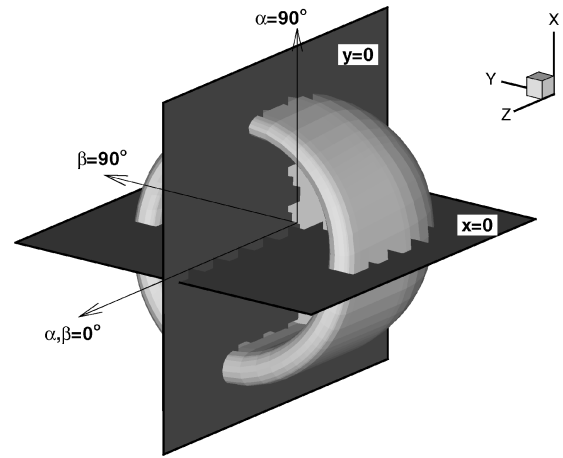

Fig. 19   Directivity definition.

Conclusions

A formulation has been proposed that permits high-order infinite elements to be applied in the time domain to predict the propagation of acoustic disturbances on unbounded irrotational mean flows.

Numerical studies have been presented to validate the formulation for simple test problems in the presence of flow.

The method has been shown also to be effective for large three-dimensional problems, provided that iterative solvers are used to advance the solution at each time step.

Application of the current scheme to a demonstration problem characteristic of tone radiation from a three-dimensional turbofan intake indicates that far-field directivity can be predicted at modest computational cost when compared to an equivalent frequency-domain computation.

Additional features, not addressed here but which would be required if the current method were to be applied to real intakes, include the following:

1) Parallel implementation: The problem size and CPU requirements for the final demonstration problem presented here are still modest compared to those for a real intake analysis at blade passing frequency, which would involve an order-of-magnitude increase in the number of degrees of freedom. Parallel implementation would then be highly desirable. The indirect solution method used here should scale efficiently in this case, but this has yet to be demonstrated.

2) Time-domain impedance boundary condition: In any real intake the effect of liners will be critical, and the implementation of a suitable time-domain impedance boundary condition would therefore be needed. A boundary condition of this type has already been applied sucessfully by other researchers to time-domain FE/IE problems in the absence of flow. This must be extended to include flow effects, via the Myers boundary condition, for real intake applications.

References

[1]Eversman, W., "Mapped Infinite Wave Envelope Elements for Acoustic Radiation in a Uniformly Moving Medium," *Journal of Sound and Vibration*, Vol. 224, No. 4, 1999, pp. 665–687.

[2]Astley, R., and Hamilton, J., "Infinite Elements for Transient Flow Acoustics," AIAA Paper 2001-2171, May 2001.

[3]Astley, R., and Hamilton, J., "Modelling Tone Propagation from Turbofan Inlets—The Effect of Extended Lip Liners," AIAA Paper 2002-2449, June 2002.

[4]Regan, B., and Eaton, J., "Application of an Efficient Iterative 3D Finite Element Scheme to the Fan Noise Radiation Problem," AIAA Paper 95-012, June 1995.

[5]Wilcox, C., "A Generalisation of the Theorems of Rellich and Atkinson," *Proceedings of the American Mathematical Society*, Vol. 7, 1956, pp. 271–276.

[6]Bettess, P., *Infinite Elements*, Penshaw, Sunderland, England, U.K., 1992.

[7]Astley, R., and Coyette, J.-P., "Conditioning of Infinite Element Schemes for Wave Problems," *Communications in Numerical Methods in Engineering*, Vol. 17, No. 1, 2001, pp. 31–41.

[8]Shirron, J., and Babuska, I., "A Comparison of Approximate Boundary Conditions and Infinite Element Methods for Exterior Helmholtz Problems," *Computer Methods in Applied Mechanics and Engineering*, Vol. 164, No. 1, 1998, pp. 121–139.

[9]Gerdes, K., and Demkowicz, L., "Solution of 3D Laplace and Helmholtz Equations in Exterior Domains Using hp-Infinite Elements," *Computer Methods in Applied Mechanics and Engineering*, Vol. 137, No. 3, 1996, pp. 239–273.

[10]Ihlenburg, F., "On Fundamental Aspects of Exterior Approximations with Infinite Elements," *Journal of Computational Acoustics*, Vol. 8, No. 1, 2000, pp. 63–80.

[11]Leis, R., *Initial Boundary Value Problems in Mathematical Physics*, Teubner, Stuttgart, Germany, 1986.

[12]Astley, R., Macaulay, G., and Coyette, J.-P., "Mapped Wave Envelope Elements for Acoustical Radiation and Scattering," *Journal of Sound and Vibration*, Vol. 170, No. 1, 1994, pp. 97–118.

[13]Saad, Y., and Schultz, M., "GMRES: A Generalized Minimal Residual Algorithm for Solving Nonsymmetric Linear Systems," *SIAM Journal on Scientific and Statistical Computing*, Vol. 7, No. 3, 1986, pp. 856–869.

[14]Van der Vorst, H., "Bi-CGSTAB: A Fast and Smoothly Converging Variant of Bi-CG for the Solution of Nonsymmetric Linear Systems," *SIAM Journal on Scientific and Statistical Computing*, Vol. 12, No. 2, 1992, pp. 631–644.

[15]Deraemaeker, A., Babuska, I., and Bouillard, P., "Dispersion and Pollution of the FEM Solution for the Helmholtz Equation in One, Two and Three Dimensions," *International Journal on Numerical Methods in Engineering*, Vol. 46, 1999, pp. 471–499.

[16]Oberai, A., and Pinsky, P., "A Numerical Comparison of Finite Element Methods for the Helmholtz Equation," *Journal of Computational Acoustics*, Vol. 8, No. 1, 2000, pp. 211–221.

[17]Free Field Technologies, *ACTRAN Rev. 2.0, Users' Guide*, Louvain-la-Neuve, Belgium, 2002.

[18]Eversman, W., "Theoretical Models for Duct Acoustic Propagation and Radiation," *Aeroacoustics of Flight Vehicles, Theory and Practise. Vol 2: Noise Control*, NASA, 1991, pp. 101–163.

[19]Tyler, J., and Sofrin, T., "Axial Flow Compressor Noise Studies," *SAE Transactions*, Vol. 70, 1961, pp. 309–332.

B. Balachandran
Associate Editor